Liver microbiota in healthy rats: the hidden inhabitants of hepatocytes

Xiao Wei Sun
Lanzhou University
Hua Zhang
Lanzhou University
Cai Yun Zhou
Lanzhou University
Wen Min Gao
Lanzhou University
Xuan Xuan Kou
Lanzhou University
Jian Gang Zhang (zhjg@lzu.edu.cn)
Lanzhou University

Research Article

Keywords: microbiota, liver, hepatocytes, intranucleus, 16S rRNA gene, healthy rats

Posted Date: April 1st, 2022

DOI: https://doi.org/10.21203/rs.3.rs-1352724/v1

Abstract

The tumor and tissue microbiomes of human beings have recently been investigated. Gut permeability was known as a possible resource for the positive detection of tissue bacteria. Herein, we report that bacteria were detected in high abundance in the hepatocyte nucleus of healthy rats, and that they were shared with gut microbiota to an extent. We assessed male Sprague Dawley (SD) rats for the 16S ribosomal ribonucleic acid (rRNA) gene. After rats were sacrificed by blood drainage from the portal vein, we extracted total deoxyribonucleic acid (DNA) from their ileal and colonic contents and liver tissues. The V3–V4 region of the 16S rRNA gene was amplified by polymerase chain reaction (PCR) and sequenced using an Illumina HiSeq 2500 platform. Sequences were assigned taxonomically by the SILVA database. We also detected bacterial lipopolysaccharide (LPS) and lipoteichoic acid (LTA) *in situ* using immunofluorescence (IF) and western blotting, and the 16S rRNA gene using fluorescent *in situ* hybridization (FISH). In the livers of six rats, we detected 54,867.50 ± 6450.03 effective tags of the 16S rRNA gene and clustered them into 1003 kinds of operational taxonomic units (OTUs; 805.67 ± 70.14, 729–893). Individuals showed conservation of bacterial richness, abundance, and evenness. LPS and the 16S rRNA gene were detected in the nuclei of hepatocytes. The main function of the annotated bacteria was correlated with metabolism (79.92 ± 0.24%). Gram negativity was about 1.6 times higher than gram positivity, but aerobic and anaerobic phenotypes were nearly the same. Liver flora also showed high expression of mobile elements, biofilm formation, and stress tolerance, as well as potentially pathogenic phenotypes. Chemoheterotrophy, fermentation, and aerobic chemoheterotrophy were the main heterotrophic functions. Liver bacteria were shared with both the small and large intestines but showed significantly higher richness, evenness, and β-diversity than the small and large intestines ($P < 0.05$). Liver flora were hidden intracellular inhabitants in healthy rat livers and were shared with gut microbiota.

Introduction

With the help of nucleotide sequencing and using the 16S ribosomal ribonucleic acid (rRNA) gene as a highly conserved marker in bacterial clades, gut microbiota—which are distributed throughout the whole gastrointestinal (GI) tract with diverse microbial communities—could be identified. Many human-sample population studies have further proven the relationship between gut microbiota (mainly fecal microbiota) alterations and the occurrence of various diseases [1–4]. Recently, researchers have found that a high-fat diet can elevate gut permeability and result in bacterial translocation from the intestine into tissues such as adipose and liver tissues [5–8]. More recently, studies have also demonstrated bacteria in various tumor cells and proposed the concept of tumor type-specific intracellular bacteria [9]. Herein, we reported bacteria in the normal liver tissues and hepatocytes of rats without dietary interference or disease development. These findings could illuminate the mechanisms of some liver diseases and the origins of gut microbiota.

Materials And Methods

Animals

Male adult Sprague-Dawley (SD) rats were used for detection. All animals received humane care, and study protocols complied with the Laboratory animal—Guideline for ethical review of animal welfare (GB/T 35892—2018) and were approved by the Medical Ethics Committee of Lanzhou University (jcyxy20190302). This study also conformed with the Animal Research: Reporting of In Vivo Experiments (ARRIVE) guidelines and Replacement, Refinement and Reduction of Animals in Research (NC3Rs).

Sample collection and contamination avoidance

Animals were anesthetized with pentobarbital sodium (5 mg/100 g body mass) followed by three skin sterilizations using 75% ethanol and iodophor. To avoid environmental contamination, all operations were conducted under a laminar-flow hood following aseptic-surgery protocols, including the use of a surgical towel, and avoided contact between skin and subcutaneous tissue. After the skin was opened, we discarded the original set of all surgical instruments and used another set. To eliminate possible blood contamination, animals were sacrificed by portal-vein blood drainage. To prevent possible fecal contamination, we began by removing liver tissues, then those of the ileum (small intestine [SI]) and colon (large intestine [LI]). Subsequently, SI and LI contents were pushed out from the outside of the gut using another set of tweezers. All samples were stored at −80°C after a quick freeze in liquid nitrogen. To avoid possible contamination during 16S rRNA gene analysis, we transported samples on dry ice to a sequencing company (BMK Co., Beijing, China), which provided an integrated service in DNA extraction, polymerase chain reaction (PCR) amplification, and sequencing via procedures that strictly avoided contamination.

Bacteria DNA extraction

We extracted total DNA from frozen liver and fecal samples (0.25–0.5 g) using a Magnetic Soil and Stool DNA Kit (#DP812; TianGen Corp., Beijing, China, https://www.tiangen.com/) per the kit protocol. All procedures were performed with sterile and disposable materials to avoid cross-contamination, including the beads.

16S PCR and sequencing library construction

We used two-round tailed PCR with the barcode at the end of primer for 16S amplification and sequencing. In the first round, the 16S rRNA gene's variable regions 3–4 (V3–V4) of interest was amplified with an initial heating step of 95ºC for 5 min, followed by 25 cycles of 30 s at 95ºC, 30 s at 50ºC, 40 s at 72ºC and a final extension step of 72ºC for 7 min. The bacterial primer was as follows: 338F: 5'-ACTCCTACGGGAGGCAGCA-3'; 806R: 5'-GGACTACHVGGGTWTCTAAT-3' [10]. The reaction system was as follows: bacterial-genome DNA, 50.0 ng ± 20%; primers (338F and 806R, 10 μM; Synbio Technologies, Suzhou, China), 0.3 μl each; KOD FX Neo Buffer (KFX-201S; TOYOBO; Biolink Biotechnology, Beijing, China, http://www.bjbiolink.com/), 5.0 μl; deoxyribose nucleotide triphosphate (dNTP; 2 mM each), 2.0 μl; KOD FX Neo, 0.2 μl; and double-distilled water (ddH_2O) added to 10.0 μl. We performed the PCR reaction using an Applied Biosystems PCR System (Veriti 96-Well 9902; Applied Biosystems, Foster City, CA, USA). PCR products (10-μl system) were purified using VAHTSTM DNA clean

beads (Vazyme Corp., Nanjing, China, http://www.vazyme.com/) at a ratio of 1:1, and eluted using 8.0–10.0 μl ddH_2O. In the second round of PCR reaction (Solexa PCR), dual-indexed sequences (barcodes) and Illumina adaptors (Illumina, Inc., San Diego, CA, USA) were added to the amplicon. The reaction system was as follows: purified V3–V4 PCR production DNA, 5.0 μl; primers (MPPI-a and MPPI-b, 2.0 μM; Synbio Technologies, Suzhou, China), 2.5 μl each; NEBNext® Ultra™ II Q5® Master Mix (New England Biolabs, Ipswich, MA, USA) (M0544L; Biolink Biotechnology, Beijing, China) 10.0 μl. The PCR reaction was performed at 98°C for 30 s, with 10 cycles of 98°C for 10 s, 65°C for 30 s, 72°C for 30 s, and an extension at 72°C for 5 min.

We detected the products using 1.8% agar gel (120 V, 40 min) and qualified them by analyzing the gel images via ImageJ software (National Institutes of Health, Bethesda, MD, USA). Next, we mixed 150 ng of each sample (samples were 1.5–14.0 μl) and purified it using an E.Z.N.A. Cycle-Pure Kit (Omega Bio-Tek, Inc., Norcross, GA, USA).

Sequencing

After quality testing on a Qsep-400 (BiOptic, Inc., New Taipei City, Taiwan, ROC) and preparation of a flow cell chip, we subjected 500 ng PCR products to paired-end (PE) sequenced on an Illumina HiSeq 2500 platform (Illumina, Inc., San Diego, CA, USA) at Biomarker Technologies Co, Ltd. (Beijing, China) according to standard protocols. The sequencing length was 350–450 bp. Original image data files were transformed into raw data (PE reads) via base calling analysis.

Quality assessment and data processing

According to the overlapping relationship, PE reads were merged with Fast Length Adjustment of SHort reads (FLASH) software v.1.2.7 (Johns Hopkins University Center for Computational Biology, Baltimore, MD, USA; raw tags) [11].We discarded tags with > 6 mismatches. The minimum overlap length was 10 bp, and the maximum mismatch ratio allowed in the overlap region was 0.2 (default). Raw tags with an average quality score < 20 in a 50-bp sliding window were then filtered using Trimmmatic software v.0.33 (USADELLAB.org) [12] and those shorter than 350 bp were removed (clean tags). We further removed possible chimeras using UCHIME v.4.2 (http://drive5.com/usearch/manual/uchime_algo.html) [13] to obtain effective tags.

Operational taxonomic-unit analysis

Effective tags were clustered at a 97% similarity level to obtain OTUs using USEARCH software v.10.0 [14]. We evaluated the α-diversity index of each sample using Mothur software v.1.30 (http://mothur.org/) and the β-diversity index using Quantitative Insights Into Microbial Ecology (QIIME) software v2.2. Degrees of similarity in species diversity between different samples were compared.

Taxonomic analysis

We compared representative OTU sequences against the Silva microbial reference database (release 128; http://www.arb-silva.de) [15]. The classification information of each OTU was obtained by comparison, and the OTU was annotated using RDPClassifier (v2.2; QIIME) [16]. Next, we counted the community composition of each sample at phylum, class, order, family, genus, and species levels. Species richness at different taxonomic levels was assessed using QIIME, and the community structure diagram of each taxonomic level was drawn using R software v3.1.1 (R Foundation for Statistical Computing, Vienna, Austria).

Immunofluorescence assays

Immunofluorescence (IF) staining was performed according to standard staining methods as described, with slight modification [5]. Briefly, we fixed frozen liver tissue sections (4 μm) with 4% paraformaldehyde for 30 min and aged them at 60°C for 10 min, followed by incubation with 0.3% Triton X-100 (#T8200; Solarbio) and 3% bovine serum albumin (BSA; B2064-50G; Sigma Germany, Munich, Germany) for 30 min. Primary antibodies (lipopolysaccharide (LPS) core, monoclonal antibody [mAb] WN1 222-5, #HM6011, 1:400 dilution; lipoteichoic acid (LTA), mAb 55, #HM2048; 1:400 dilution; both from Hycult Biotech, Uden, Netherlands) or phosphate-buffered saline (PBS; #BL601A; BioSharp Life Sciences, Hefei, China) as negative control were applied to slides overnight at 4˚C; secondary antibody (DyLight 488 goat anti-mouse immunoglobulin G [IgG]; Ex/Em = 493/518 nm, #AMJ-AB2004; 1:800 dilution; AmyJet Scientific Inc., Wuhan, China) were added for 1 h at 37°C. We counterstained the slides with 4',6-diamidino-2-phenylindole (DAPI; 0.5 mg/ml; Ex/Em = 364/454, #BL105A; BioSharp) at room temperature (RT) for 10 min, and then dried the slices in a dark room and mounted them with an anti-fluorescence attenuator mountant. Paraformaldehyde fixed *Staphylococcus* and *Escherichia coli* (preserved and kind gifts from Professor Jian Han (Lan Zhou University, China) were used as Gram-positive and Gram-negative controls, respectively. We observed and recorded slides using Nikon-ECLIPSE 80i/DS-Ri2/NIS-ElementsD microscopy (Nikon, Tokyo, Japan).

Equipment and settings

Images were captured with software NIS-Elements D using an Nikon-ECLIPSE 80i upright fluorescence microscope outfitted with a Nikon DS-Ri2 camera, Plan Fluor 40x DIC M N2 objectives (objective numerical aperture: 0.75, refractive index: 1.000). The images were acquisited with 96 dpi in x- and y-axis with 4908 × 3264 pixel dimensions, and the image bit depth was 24.

16S rRNA gene fluorescent *in situ* hybridization

We detected the 16S rRNA gene in tissues according to the instructions of a EUB338 FISH Probe Kit (#20 μM; FBPC-10; Creative Bioarray, Shirley, NY, USA). Briefly, frozen tissue slides (4 μm) were fixed with 4% paraformaldehyde for 30 min and at 60°C for 10 min, followed by incubation with 0.3% Triton X-100 for 30 min. We then incubated slides in lysozyme at 37°C for 15 min. As a positive control, a bacteria smear was incubated in 0.01 M HCl at RT for 20 min. Slides were fixed with 4% paraformaldehyde for another 15 min at RT, after which we treated them with diethyl pyrocarbonate (DEPC) for 10 min and incubated

them with BSA (3%) for 2 h. BSA was then discarded, and fluorescein isothiocyanate (FITC)–labeled probes (EUB338 GCTGCCTCCCGTAGGAGT) and a non-specific complement probe (nEUB338 CGACGGAGGG CATCCTCA; #FBPC-13; Creative Bioarray) were hybridized in a pre-warmed humidified hybridization chamber and incubated overnight at 39˚C (range, 38–42°C). We diluted FISH probe EUB338 or nEUB338 with 35% hybridization buffer (1:100), denatured it at 84°C for 5 min, and then incubated at 37°C for 3 min. After hybridization, we carefully removed the sealing film by soaking the slides in wash solution (WS; 2 × saline-sodium citrate [SSC]/0.1% Tween 20) at RT for 15 min to loosen the coverslips. Slides were then rinsed twice in WS for 15 min each time, immersed in 75% and 100% ethanol for 2 min, and then air-dried for 20 min. We counterstained slides with DAPI antifade solution (using EUB338 FISH Probe Kit) for 10 min and examined them under the Nikon fluorescence microscope.

LPS and LTA western blotting

We separated cytoplasmic from nuclear components using a Minute Cytoplasmic and Nuclear Fractionation Kit (#sc-003; Invent, Beijing, China). The liver tissue was washed with pre-cooled sterile PBS, and 60 mg of fresh (or frozen) soft liver tissue was added to a 1.5-ml sterile microcentrifuge tube. We then added 200 μl of pre-cooled sterile PBS to the same tube and ground tissue with a clean plastic grinding rod for 2–3 min on ice until no solid tissue was visible, after which the frozen liver tissue sample was thawed completely on ice and then ground again. After incubation on ice for 5 min, we carefully transferred the supernatant into another pre-cooled sterile 1.5-ml microcentrifuge tube. Cells were harvested from the suspension by low-speed centrifugation (500 × g) at 4°C for 3 min. We added 200 μl cytoplasmic extraction buffer for every 20 μl of cell volume, vortexed the tube vigorously for 15 s, and incubated it on ice for 15 min. Then, we centrifuged it for 5 min at 16000 × g and 4°C in a microcentrifuge. The supernatant (cytosol fraction) was transferred to a fresh pre-chilled 1.5-ml tube; the pellet was washed in 0.5 ml cold PBS, centrifuged at 8000 × g for 5 min to reduce contamination of cytosolic proteins and frozen at −80°C. We added 100 μl nuclear extraction buffer to the pellet (ratio of cytoplasmic to nuclear extraction buffer, 2:1), vortexed the mixture vigorously for 30 s and incubated the tube on ice for 2 min; this sequence of steps was repeated five times. Immediately afterward, we transferred the nuclear extract to a pre-chilled filter cartridge via a collection tube and centrifuged it at 16000 × g in the microcentrifuge for 30 s at 4°C. We discarded the filter cartridge and stored the nuclear extract at −80°C. The bicinchoninic acid (BCA) method was used to measure protein concentrations. Protein samples were separated by sodium dodecyl sulfate polyacrylamide gel electrophoresis (SDS-PAGE; 12% separating gel), transferred onto a polyvinylidene difluoride (PVDF) membrane (MilliporeSigma, Burlington, MA, USA) , and probed with the above-indicated primary antibodies at 4°C overnight, followed by the appropriate secondary horseradish peroxide (HRP)–conjugated IgG antibody at RT for 1 h. The following antibodies were used: primary, LPS (1:400; HM6011; Hycult), LTA (1:1000; #HM2048; Hycult), Lamin-B1 (1:2000, #ab16048; Abcam, Cambridge, UK), glyceraldehyde 3-phosphate dehydrogenase (GAPDH; 1:4000; #YM3215; Proteintech, Chicago, IL, USA); secondary, HRP-labeled goat anti-rabbit (1:5000, #RS0002; ImmunoWay Biotechnology Co., Plano, TX, USA) and HRP-labeled goat anti-mouse (1:5000; #RS0001; ImmunoWay). Protein bands were visualized using an

electrochemiluminescence (ECL) kit (Super ECL Detection Reagent, Yeasen Biotechnology Co., Ltd., Shanghai, China) and ImageJ software v6.0.

Statistical analysis

All data were expressed as mean ± standard deviation. We conducted all statistical analyses using SPSS software v19.0 (IBM Corp., Armonk, NY, USA). An independent-sample *t*-test was used for comparisons between two groups, and one-way analysis of variance (ANOVA) was used for mean comparisons between groups. Differences were considered statistically significant at $P < 0.05$.

Results

Liver microbiota detected by 16S rRNA gene sequencing

We sequenced the V3–V4 region of the 16S rRNA gene in liver tissues, obtaining 54,867.50 ± 6,450.03 effective tags (Table S1). These tags were further clustered into 1003 kinds of OTUs (805.67 ± 70.14, 729–893), of which six rats shared 598 kinds of OTUs. Annotated species numbers at different levels are summarized in Table S2. Individuals showed obvious conservation of bacterial abundance (tags), richness (OTU number), and evenness (Table 1). The coefficient of variation (CV) of the α-diversity index was low.

Table 1
Alpha diversity among individual liver samples

Sample	Ace	Chao	Shannon	Simpson
A5	920.47	936.60	8.02	0.99
A12	737.07	735.90	7.94	0.99
A29	906.05	921.79	8.08	0.99
A32	868.85	878.24	8.03	0.99
A36	797.98	810.00	8.06	0.99
A46	749.48	760.69	7.90	0.99
CV	0.096	0.100	0.009	0.001

CV, coefficient of variation, calculated as standard deviation (SD) divided by mean. Simpson index was calculated as 1 - $\sum pi^2$.

At the phylum level, liver microbiota were annotated and clustered into 19 species. No exclusive species was observed among individuals. Firmicutes, Proteobacteria, Bacteroidetes, Acidobacteria, Actinobacteria, Chloroflexi, Verrucomicrobia, Spirochaetes, Cyanobacteria, and Gemmatimonadetes were

the top 10 dominant bacteria in these rats (Fig. 1). CV ranged from 0.21 to 0.42 (Table S3). Flora annotation at the genus level is provided in Table S4.

Liver flora detected *in situ*

To prove the existence and locations of bacteria in the liver, we further performed histological bacteria detection *in situ*. We conducted IF using antibodies against bacterial LPS and LTA to detect Gram-negative and -positive bacteria, respectively [5]. We also used RNA FISH with a universal probe against the bacterial 16S rRNA gene (EUB338) to detect bacterial RNA in the liver [5]. To control for nonspecific staining, IF-negative controls (no primary antibody) and FISH-negative controls (nEUB338) were also applied to the samples. Bacterial LPS and 16S rRNA were positive in the liver and located in the nuclei of hepatocytes. LTA was not detected (Fig. 2). We then separated the cytoplasmic and nuclear components of liver tissue and detected the expression of LPS and LTA. The results confirmed the nuclear location of LPS (Fig. 3).

Functional analysis of liver bacteria

According to a Kyoto Encyclopedia of Genes and Genomes (KEGG) database comparison using the Phylogenetic Investigation of Communities by Reconstruction of Unobserved States 2 (PICRUSt2) algorithm and the tax4fun package in R, the main function of annotated liver bacteria was related to metabolism (79.92 ± 0.24%). Genetic information processing (6.31 ± 0.10%), environmental information processing (6.29 ± 0.12%), and cellular processes (3.49 ± 0.08%) were less dominant and showed no obvious harm to the body (2.58 ± 0.06%). Moreover, the organismal-system function (1.41 ± 0.02%) was low (Table S5).

According to BugBase analysis, liver bacteria possessed diverse phenotypes. The Gram-negative phenotype was about 1.6 times more common than the Gram-positive one, but the aerobic and anaerobic phenotypes were nearly equally common. Moreover, liver flora also showed high expression of mobile elements, biofilm formation, and stress tolerance as well as potentially pathogenic phenotypes (Table S6). According to faprotax analysis, the liver bacteria were mainly heterotrophic by functions of chemoheterotrophy (36.21 ± 0.88%), fermentation (20.33 ± 1.61%), and aerobic chemoheterotrophy (15.41 ± 0.93%; Table S7).

Relationship between liver and gut microbiota

The relationship between the microbiota of the liver and gut was extremely interesting. Therefore, we compared the 16S rRNA gene sequencing data of liver flora with those of fecal and ileal flora. Liver microbiota shared a large percentage of bacteria with those of the ileum and feces (Fig. 4). Except for abundance distinction, phylum species distribution showed no difference (Table S8). At the genus level, among 337 flora, only two bacteria (*Psychrobacter* and *Leptolyngbya_VRUC_135*) were liver exclusive and three (*uncultured bacterium o Rhodospirillales*, *Muribacter*, and *uncultured bacterium f Rs-E47 termite*

group) were exclusive to the SI and LI (Table S9), indicating remarkable homogeneity of the liver and gut microbiota.

As shown by α-diversity analysis, richness and evenness in individuals were significantly higher than in the SI or LI ($P < 0.05$; Fig. 5A–B, Table S10). According to the β-diversity analysis, liver flora exhibited significantly higher similarity than intestinal flora (Fig. 5C–F). The visceral bacteria are widely considered to originate from the gut microbiota via gut leakage of colonic mucosa (the "gut-to-liver axis"). However, the similarity of liver microbiota among different individuals being greater than the distance between gut and liver (Fig. 5C–F) seemed to throw this concept into doubt. We then compared the bacteria of the liver with those of the intestine. Liver bacteria showed significantly higher richness than intestinal bacteria from phylum to species level ($P < 0.05$; Table S11). We compared liver bacteria individually against gut microbiota. In each animal, a large number of liver bacteria were exclusive to the liver in comparison with the animal's ileal- and fecal-exclusive bacteria (genus level, liver: 113.67 ± 83.32 *vs.* ileum: 4.67 ± 2.58 or feces: 12.00 ± 8.15; $P < 0.05$). Moreover, liver–ileum and liver–ileum–feces shared bacteria (107.67 ± 83.73 and 71.33 ± 11.78, respectively) were significantly more numerous than liver–feces shared bacteria (14.00 ± 9.44; Fig. S1, Table S12). We also calculated the distance between liver and intestinal samples by the binary Jaccard method. The liver was significantly closer to the ileum than to feces (liver to liver: 0.09 ± 0.02; liver to ileum: 0.44 ± 0.25; liver to feces: 0.74 ± 0.03; $P < 0.05$; Fig. 6, Table S13). These relatively independent phenomena challenged the concept of the "gut-to-liver axis," suggesting instead an upstream "liver-to-gut axis" and the possibility of bacterial translocation from the liver to gut.

Discussion

To our knowledge, this is the first report of liver microbiota as the normal component of hepatocytes. With the help of metagenomic sequencing, we identified the existence of bacteria in liver tissues of SD rats. We repeated the 16S rRNA gene sequencing experiment three times on two sequencing platforms (Beijing Biomarker Technologies Co., Ltd., www.biomarker.com.cn, Project Number: BMK191202–X098–01, BMK200916–AC763–0101, and Shanghai Bioprofile Technology Co., Ltd., Shanghai, China, www.bioprofile.cn, Project Number: BP20123) in ordinary or clean rats (data not shown) and repeated the in situ detection in clean rats more than three times. All results were consistent. Because the sequencing of the 16S rRNA gene's V3–V4 region is a mature technique and strictly controlled process, and because the technique for annotation of bacteria has been tested and widely used, these results were credible.

Bacteria in liver tissues were high in richness and abundance. A total of 1003 kinds of OTU were identified in six rats with 54,867.50 ± 6450.03 effective tags. Their α-diversity was even higher than that of intestinal bacteria. The most striking features of liver bacteria might be the conservation of richness, abundance, and evenness and higher similarity among different individuals compared to gut bacteria.

We further confirmed the results by LPS/LTA and EUB338 detection *in situ*. We found that bacteria were located in the nuclei of hepatocytes were well organized. Unlike LPS and EUB338, LTA was not detectable. We hypothesized that LTA might be a less sensitive biomarker for detection of Gram-positive bacteria in

hepatocytes, or that such bacteria in hepatocytes might differ structurally from environmental Gram-positive bacteria (*e.g.*, lacking expression of LTA), because functional analysis showed that liver bacteria were highly Gram-positive and showed high percentage of chemoheterotropy, fermentation, and aerobic chemoheterotrophy. After we isolated liver tissues into the cytoplasm and nuclear components, Western blot also proved there was strong expression of LPS in the latter, with negative in the former. LTA was not detected in both types of components.

After the identification of liver bacteria, two key questions might arise: (1) where are the bacteria from, and (2) what functions do they have and by what mechanisms are they performed? The visceral bacteria have long been considered to come from the gut microbiota through the mechanism of gut leakage. In this study, the liver microbiota did share bacteria with the gut microbiota, with only a few exclusive bacteria. However, in each individual, a large proportion of liver bacteria were exclusive when compared with its gut microbiota counterparts. Gut microbiota showed variation and dynamic changes caused by diet and environment, whereas liver microbiota remained constant; thus, this exclusivity can be acceptable to some extent. However, the question remains: why were the liver microbiota of different individuals significantly more similar than the gut microbiota to the liver microbiota—that is, why was microbiota composition among different individuals more similar than liver microbiota to its gut counterpart?

In this study, liver bacteria showed significantly higher α-diversity than intestinal bacteria. Even if bacteria were from the gut microbiota, how and when did they enter the liver and locate themselves in the nucleus in a well-organized manner in healthy individuals? These findings suggest inherent features of liver microbiota.

The roles of liver microbiota are also unknown. According to annotation, the functions of liver bacteria were primarily metabolic rather than those that would harm the host. This was consistent with the characteristics of native bacteria. In terms of whether these were parasitic or symbiotic, and whether these bacteria were involved in the regulation of gene expression or cell life activities, we found that the question of the origin of life may be involved. This should be further proven the way the existence of oncogenes was. Furthermore, as far as the harm to the body is concerned, are the liver bacteria associated with the development of various metabolic diseases, such as steatosis, insulin resistance, or hepatic cancer?

In conclusion, we found that liver microbiota existed in the nuclei of hepatocytes, of which they might be inherent inhabitants. The sources and functions of these bacteria in cell life activities and disease development should be investigated in the future.

Abbreviations

SD: Sprague Dawley; 16S rRNA: 16S ribosomal ribonucleic acid; DNA: deoxyribonucleic acid; GI: gastrointestinal; SI: small intestine; LI: large intestine.

Declarations

Ethics approval and consent to participate

All methods were carried out in accordance with relevant guidelines and regulations of the Laboratory animal—Guideline for ethical review of animal welfare (GB/T 35892—2018) and all experimental protocols were approved by the Medical Ethics Committee of Lanzhou University (jcyxy20190302). All methods were reported in accordance with ARRIVE guidelines (https://arriveguidelines.org) for the reporting of animal experiments.

Consent for publication

Not applicable.

Availability of data and materials

The raw datasets generated during the current study are available in the NCBI repository (https://www.ncbi.nlm.nih.gov/), BioProject: PRJNA820028.

Competing interests

The authors declare that they have no competing interests.

Funding

A grant from the National Natural Science Foundation of China (NSFC; No. 81670776) to JGZ.

Authors' contributions

JGZ contributed to the study concept and design. XWS and JGZ contributed to the analysis and interpretation of data and drafted the manuscript. HZ completed the detection *in situ*. All authors contributed to the acquisition of data and critical revisions of the manuscript. All authors approved the final manuscript prior to submission. XWS and HZ shared co-first authors, XWS and JGZ shared co-corresponding authors.

Acknowledgments

We thank LetPub (www.letpub.com) for its linguistic assistance during the preparation of this manuscript.

References

1. Patterson E, Ryan PM, Cryan JF, Dinan TG, Ross RP, Fitzgerald GF, et al. Gut microbiota, obesity and diabetes. Postgrad Med J. 2016;92:286–300.

2. Gomaa EZ. Human gut microbiota/microbiome in health and diseases: a review. Antonie Van Leeuwenhoek. 2020;113:2019–2040.
3. Roy Sarkar S, Banerjee S. Gut microbiota in neurodegenerative disorders. J Neuroimmunol. 2019;328:98–104.
4. Schoeler M, Caesar R. Dietary lipids, gut microbiota and lipid metabolism. Rev Endocr Metab Disord. 2019;20:461–472.
5. Amar J, Chabo C, Waget A, Klopp P, Vachoux C, Bermúdez-Humarán LG, et al. Intestinal mucosal adherence and translocation of commensal bacteria at the early onset of type 2 diabetes: molecular mechanisms and probiotic treatment. EMBO Mol Med. 2011;3:559–572.
6. Massier L, Chakaroun R, Tabei S, Crane A, Didt KD, Fallmann J, et al. Adipose tissue derived bacteria are associated with inflammation in obesity and type 2 diabetes. Gut. 2020; 69:1796–1806.
7. Burcelin R, Serino M, Chabo C, Garidou L, Pomié C, Courtney M, et al. Metagenome and metabolism: the tissue microbiota hypothesis. Diabetes Obes Metab. 2013;15 Suppl 3:61–70.
8. Anhê FF, Jensen BAH, Varin TV, Servant F, Van Blerk S, Richard D, et al. Type 2 diabetes influences bacterial tissue compartmentalisation in human obesity. Nat Metab. 2020;2:233–242.
9. Nejman D, Livyatan I, Fuks G, Gavert N, Zwang Y, Geller LT, et al. The human tumor microbiome is composed of tumor type-specific intracellular bacteria. Science. 2020; 368:973–980.
10. Chen K, Luan X, Liu Q, Wang J, Chang X, Snijders AM, et al. Drosophila histone demethylase KDM5 regulates social behavior through immune control and gut microbiota maintenance. Cell Host Microbe. 2019;25:537–552.e8.
11. Yang C, Xu Z, Deng Q, Huang Q, Wang X, Huang F. Beneficial effects of flaxseed polysaccharides on metabolic syndrome via gut microbiota in high-fat diet fed mice. Food Res Int. 2020;131:108994.
12. Bolger AM, Lohse M, Usadel B. Trimmomatic: a flexible trimmer for Illumina sequence data. Bioinformatics. 2014; 30:2114–2120.
13. Edgar RC, Haas BJ, Clemente JC, Quince C, Knight R. UCHIME improves sensitivity and speed of chimera detection. Bioinformatics. 2011;27:2194–2200.
14. Edgar RC. UPARSE: highly accurate OTU sequences from microbial amplicon reads. Nat Methods. 2013;10:996–998.
15. Quast C, Pruesse E, Yilmaz P, Gerken J, Schweer T, Yarza P, et al. The SILVA ribosomal RNA gene database project: improved data processing and web-based tools. Nucleic Acids Res. 2013;41:D590-596.
16. Wang Q, Garrity GM, Tiedje JM, Cole JR. Naive Bayesian classifier for rapid assignment of rRNA sequences into the new bacterial taxonomy. Appl Environ Microbiol. 2007;73:5261–5267.

Figures

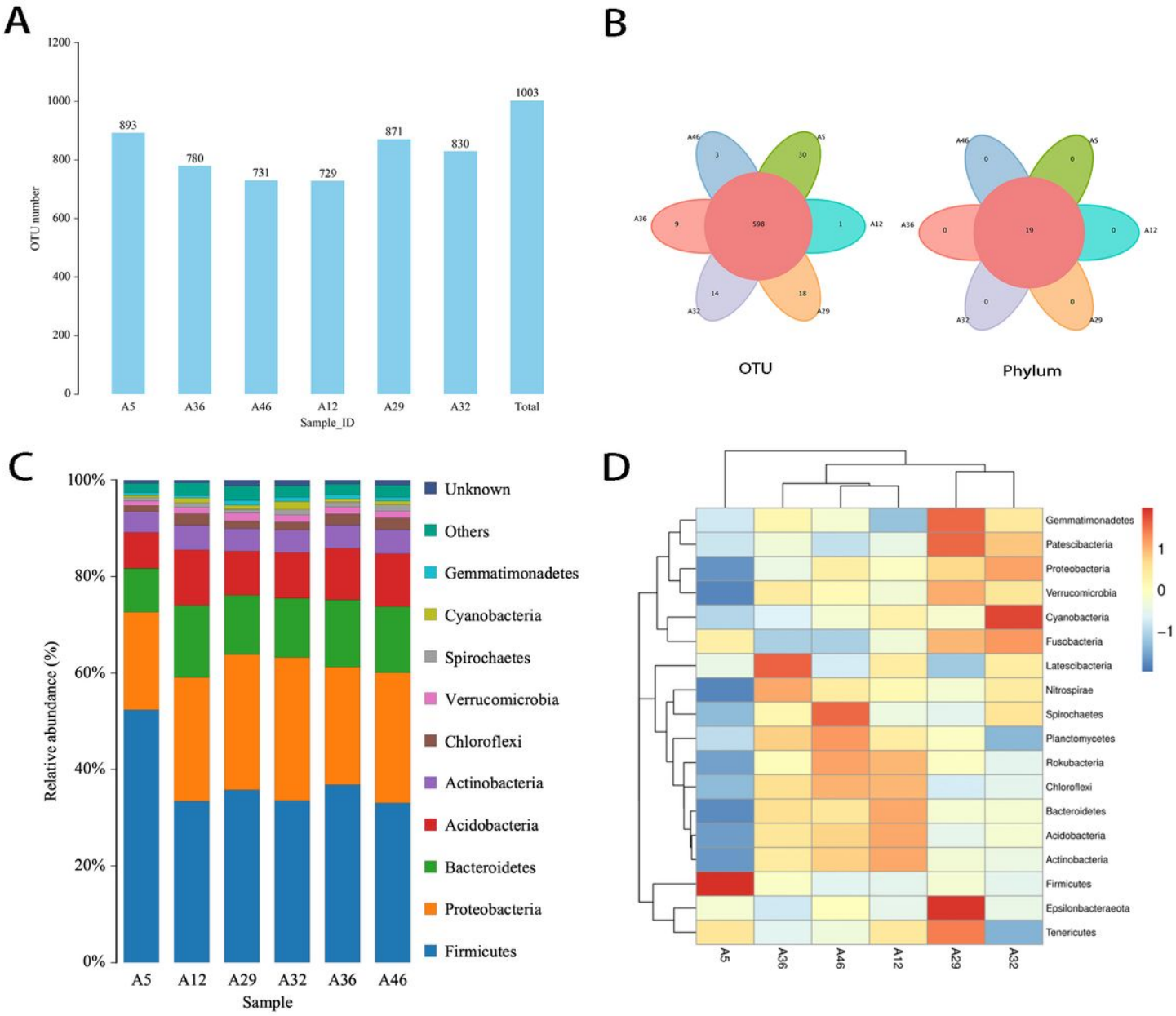

Figure 1

OTU distribution and taxonomy in liver microbiota (phyla). (A) OTU number of samples. (B) Venn diagram. (C) Species distribution (phyla). (D) Abundance heatmap (phyla).

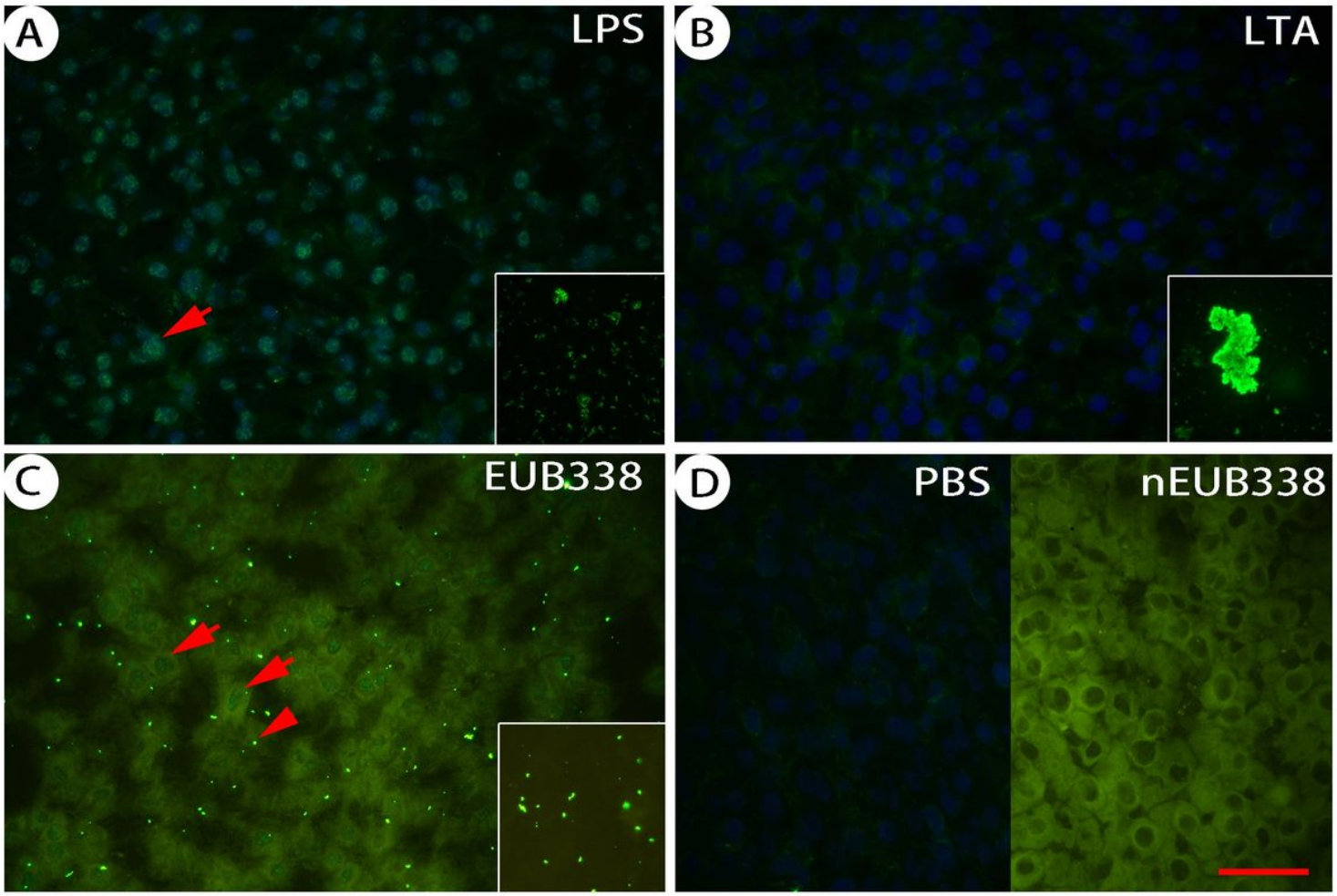

Figure 2

LPS and 16S rRNA were detected in hepatocytes. (A) LPS was detected in the nuclei of hepatocytes (arrow). Insert box: positive control of LPS with *E. coli*. (B) LTA was not detected in hepatocytes. Insert box: positive control of LTA with *Staphylococcus aureus*. (C) We detected 16S rRNA with EUB338 in the nuclei of hepatocytes (arrow). Randomly distributed bacteria contamination can be found as a positive control (arrowhead). Insert box: positive control of 16S rRNA with *S. aureus*. (D) Negative control of IF (PBS) and FISH (nEUB338). Green, FITC labeling; blue, DAPI counterstaining. LPS: lipopolysaccharide, LTA: lipoteichoic acid. Bar = 50 μm. FITC labeling and DAPI counterstaining images were merged with software NIS-Elements D. The exposure time was 700 ms.

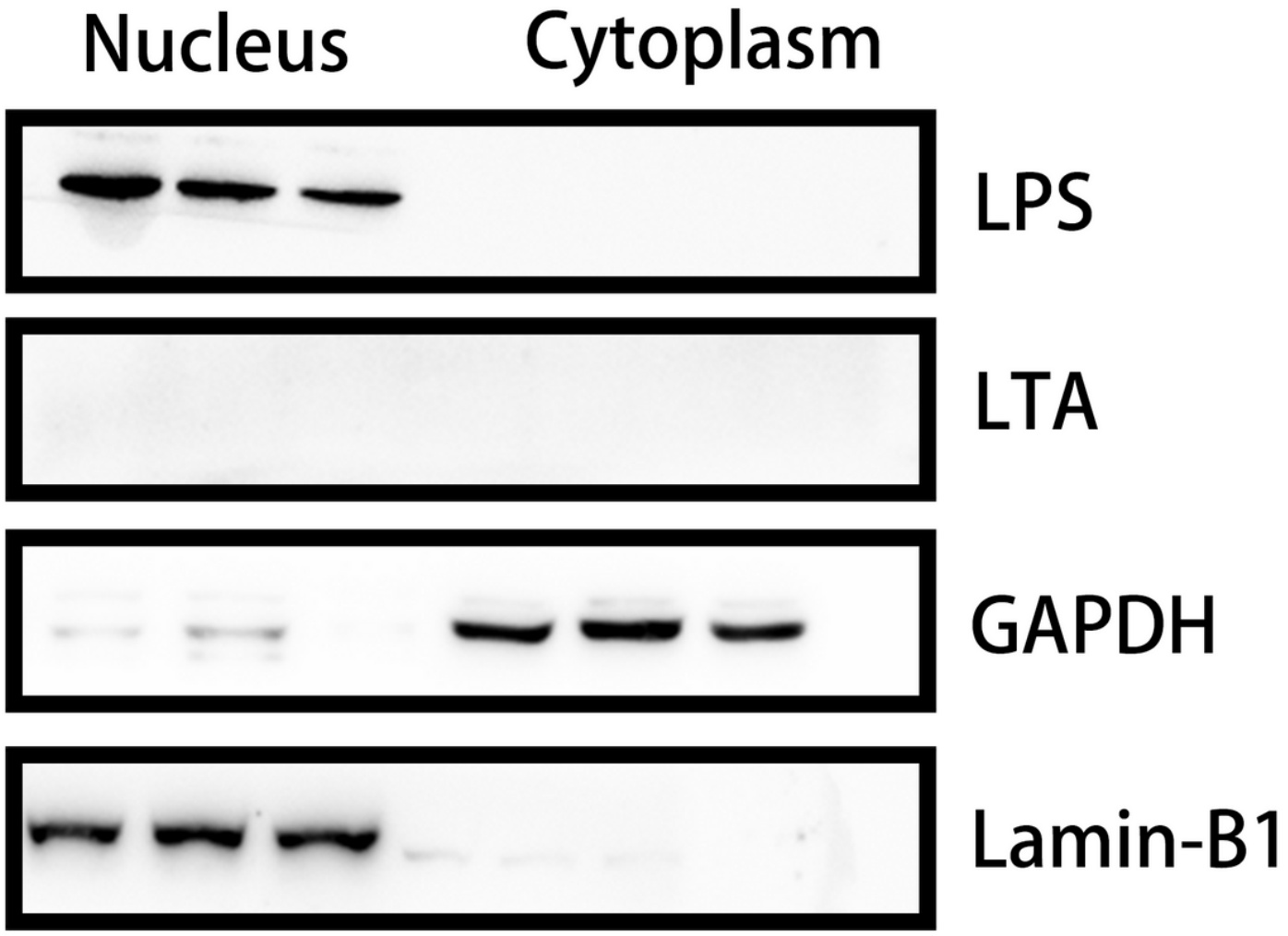

Figure 3

LPS was positive in the nuclear fraction of liver tissues. Western blotting determined expression patterns of tested LPS in rat livers. Gels/blots were cropped from different parts of the same gel.

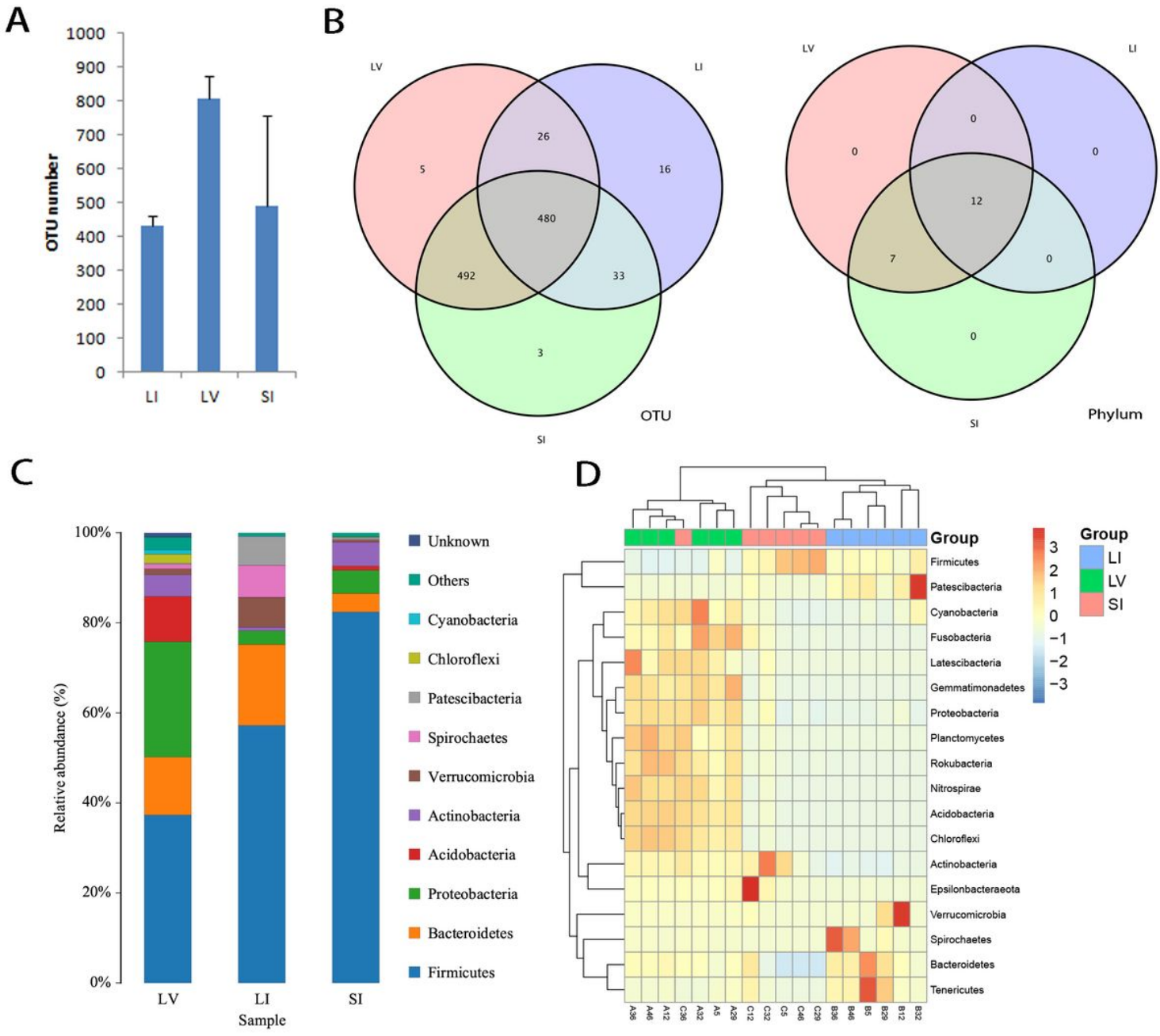

Figure 4

OTU distribution and taxonomy in liver, ileum, and feces. (A) OTU distribution of samples. (B) Venn diagram of phyla shows shared and exclusive bacteria. (C) Species distribution (phyla). (D) Abundance heatmap (phyla). Bacterial abundance: top 20; abundance ratio > 1%; distance calculation, Euclidean; cluster calculation, complete. LV, liver; LI, large intestine (feces); SI, small intestine (ileum).

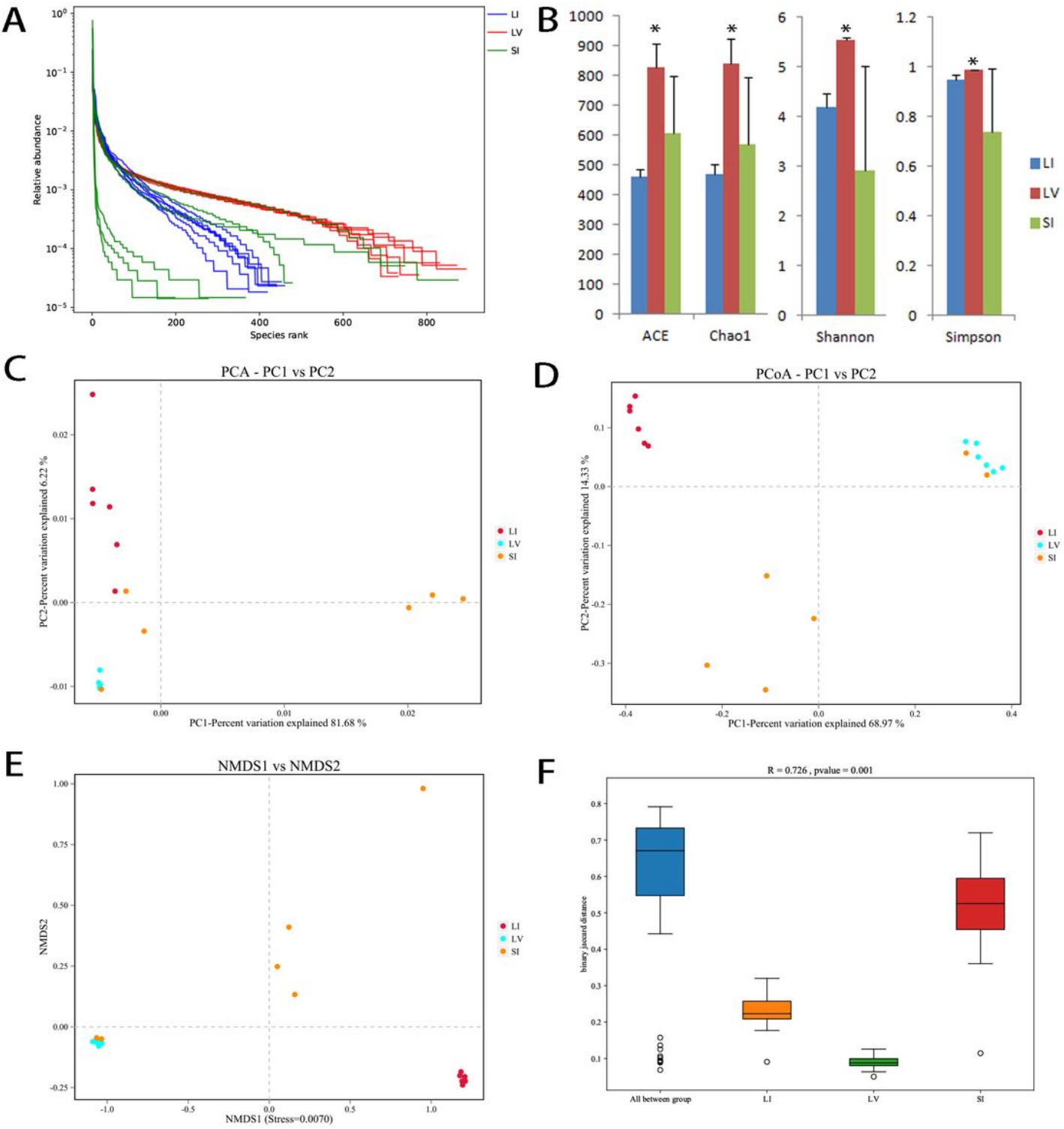

Figure 5

Alpha and beta diversity in liver and intestinal-bacteria composition. Liver bacteria showed significantly higher richness and evenness than gut bacteria. (A) Rank abundance curve of liver and intestinal bacteria. (B) Indices of α-diversity. *: compared with SI and LI, $P < 0.05$. Simpson index was calculated as $1-\sum pi^2$. Similarity across different individuals was also higher than the intestine bacteria (genus level,

binary Jaccard method). (C) Principal-components analysis (PCA). (D) Principal-coordinate analysis (PCoA). (E) Non-metric multidimensional scaling (NMDS) analysis. (F) Analysis of similarity (ANOSIM).

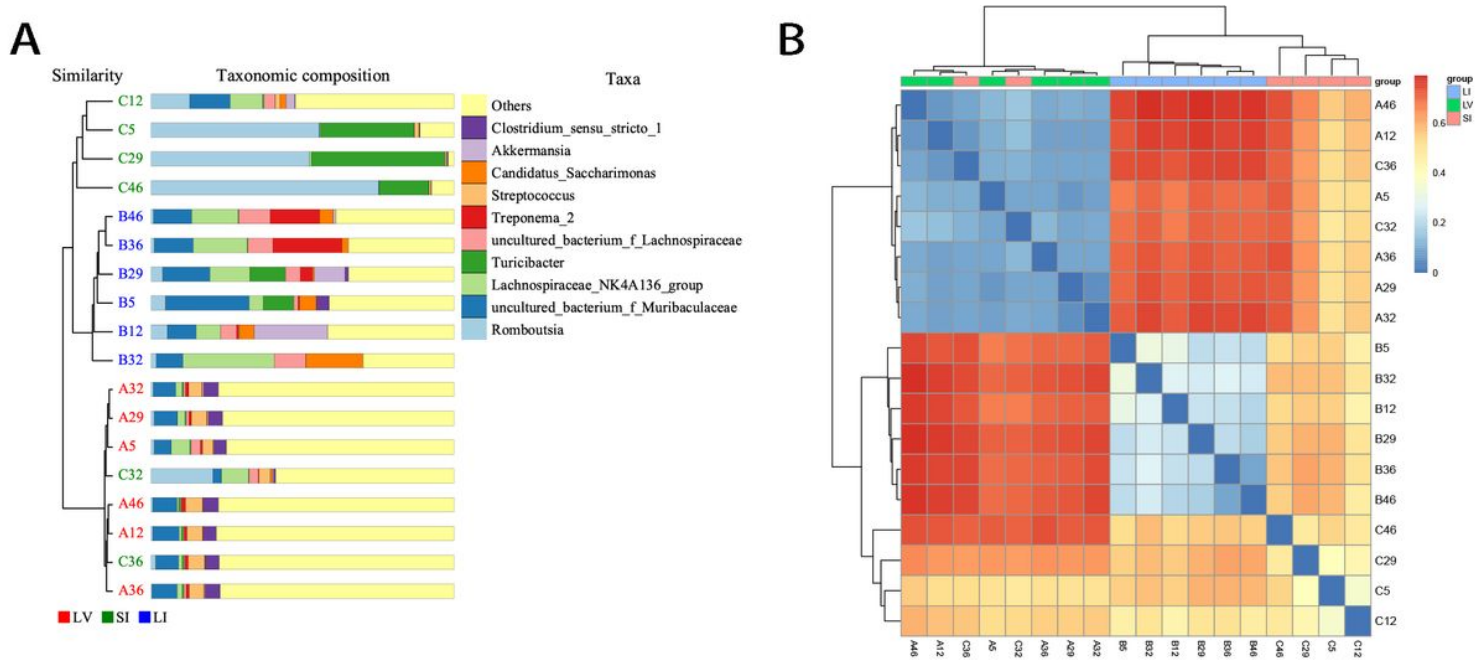

Figure 6

Relationship between liver and intestinal bacteria. The distance from the liver to the small intestine was smaller than that from the liver to the large intestine (genus level, binary Jaccard method). (A) Unweighted pair group method with arithmetic mean (UPGMA) analysis. (B) Distance heatmap between samples.

Supplementary Files

This is a list of supplementary files associated with this preprint. Click to download.

- SupplementaryTable13581011.doc
- SupplementaryTable1213FigureS1.doc
- SupplementaryTable4.doc
- SupplementaryTable9.doc
- originaldigitalimages.pdf
- graphicabstract.jpg